NASA TECHNICAL MEMORANDUM 102592
AVSCOM TECHNICAL MEMORANDUM 90-B-003

STRAIN ENERGY RELEASE RATE ANALYSIS OF DELAMINATION IN A TAPERED LAMINATE SUBJECTED TO TENSION LOAD

S. A. Salpekar, I. S. Raju, and T. K. O'Brien

March 1990

NASA

National Aeronautics and
Space Administration

Langley Research Center
Hampton, Virginia 23665

US ARMY
AVIATION
SYSTEMS COMMAND
AVIATION R&T ACTIVITY

SUMMARY

A tapered composite laminate subjected to tension load was analyzed using the finite element method. The $\{[0_7/(\pm45)]/_\uparrow[(\pm45)_3]/[0/(\pm45)/0]\}_s$ glass/epoxy laminate has a $(\pm45)_3$ group of plies dropped in three distinct steps, each 20 ply-thichnesses apart, thus forming a taper angle of 5.71 degrees. Steep gradients of interlaminar normal and shear stress on a potential delamination interface suggest the existence of stress singularities at the points of material and geometric discontinuities created by the internal plydrops. The delamination was assumed to initiate at the thin end of the taper on the -45/+45 interface indicated by the arrow in the laminate layup and the delamination growth was simulated in both directions, i.e. along the taper and into the thin region. The total strain-energy-release rate, G, and the mode I and mode II components of G, were computed at the delamination tips using the virtual crack closure technique. In addition, G was calculated from a global energy balance method. The strain-energy-release rate for a delamination growing into the thin laminate consisted predominantly of mode I (opening) component. For a delamination growing along the tapered region, the strain-energy-release rate was initially all mode I, but the proportion of mode I decreased with increase in delamination size until eventually total G was all mode II. The total G for both delamination tips increased with increase in delamination size, indicating that a delamination initiating at the end of the taper will grow unstably along the taper and into the thin laminate simultaneously.

INTRODUCTION

Composite rotor hubs are currently being designed and manufactured that are hingeless and bearingless to reduce weight, drag, and the number of parts in the hub. Such a design would involve tapering the laminate by dropping some plies in the flexure region of the hub. The plydrop in the laminate creates geometric and material discontinuities that create large interlaminar stresses and initiate delaminations. Therefore, there is a need to analyze tapered laminates with ply drops to understand their failure mechanisms. However, only a limited amount of literature is available on tapered laminates.

Adams et. al. [1] analyzed a $[0_{16}/(\pm45)_5/90_4]$ graphite/epoxy laminate in which two zero degree plies were dropped. The effect of compressive load, moisture, and temperature due to the presence of the plydrop was studied using a 3-D finite element analyses with nonlinear orthotropic response. They concluded that all the interlaminar stresses induced by a 0 degree ply drop-off anywhere in the laminate were negligible compared to the in-plane stresses. However, they did not account for the low interlaminar strength of the composite compared to the in-plane strength.

Cannon [2] conducted experiments on graphite/epoxy tapered laminates from the $[\pm45/0]_s$ and $[\pm15/0]_s$ families, subjected to tension load. For most laminates the failure mode and the failure stress were similar to that of the untapered specimen at the thin (dropped) end of the laminate. An analysis based on the minimization of total potential energy which accounted for the effect of eccentricity due to the plydrop was used to predict the in-plane failure stresses in unsymmetric laminates. The tests on

$[\pm 45/0/(\pm 45/0)_D]_s$, where D denotes dropped plies, showed that dropping a number of plies lumped together can change the initial damage from in-plane failure to delamination.

Kemp and Johnson [3] analyzed a tapered beam having a single plydrop using the finite element method. Symmetric and unsymmetric laminates were modeled as a generalized plane deformation problem subjected to a uniform strain in the longitudinal direction. The layups considered were $(\pm 45/0/90/0_{nD}/90/0/\pm 45)_T$ and $(0/90/\pm 45/0_{nD}/\pm 45/90/0)_T$ where n, the number of dropped zero degree plies, was chosen to be 1, 2, or 3. Failure strains were calculated corresponding to resin failure at the dropped plies, based on a maximum principal stress criterion. Alternatively the failure strains were obtained for intralamina failure in tension and compression, using the Tsai-Wu criterion. The first failure event in tension or compression was predicted to occur in the resin.

Although the stress distributions in the laminate help to identify the highly stressed critical areas, maximum stress or strain criteria cannot be used to predict delamination onset and growth if the stresses are singular. However, interlaminar fracture toughness, which is generic to a given composite material, can be used to predict the loads corresponding to the onset and propagation of delamination [4,5,6]. For example, delamination growth can be predicted from the mode I and mode II components of the strain-energy-release rate under static loading and from the total strain-energy-release rate for fatigue loading [5,7]. Therefore, the purpose of this paper is to study the interlaminar stress distributions in a tapered beam subjected to tension loads and to determine the strain-energy-release rate for delamination growth that may occur due to the presence of plydrops.

A typical stacking sequence used in a helicopter hub is $\{[0_9]/[(\pm45)_3]/[(\pm45)_2]\}_s$. The laminate considered here is a $\{[0_7/(\pm45)]/\uparrow$ $[(\pm45)_3]/[0/(\pm45)/0]\}_s$ tapered laminate. This laminate has the same number of $0°$ and $\pm45°$ plies as the hub but a somewhat different stacking sequence. The $(\pm45)_3$ plies are dropped in three steps, 20 ply thicknesses apart. The dropped plies result in a taper angle of $5.71°$. The laminate was analyzed using a two-dimensional finite-element analysis. The interlaminar normal and shear stress distributions along the taper interface, indicated by an arrow in the above layup, are presented. Delaminations are assumed to initiate at the point of highest interlaminar stress along this interface. The mode I, mode II and total strain-energy-release rates for various delamination lengths are presented. These results were used to hypothesize the stability of delamination growth under static and fatigue loading.

NOMENCLATURE

a	delamination length along taper
b	delamination length in the thin region
E_{11}, E_{22}, E_{33}	Young's moduli
G	total strain-energy-release rate
G_I, G_{II}, G_{III}	mode I, mode II, and mode III components of strain-energy-release rate, respectively
G_{12}, G_{13}, G_{23}	shear moduli
h	ply thickness
N_x	total load per unit width on symmetric half laminate

x	distance along delaminations
X, Y, Z	Cartesian coordinates
σ_o	uniform tension load per unit area
σ_n	interlaminar normal stress
τ_{nt}	interlaminar shear stress
$\nu_{12}, \nu_{13}, \nu_{23}$	Poisson's ratios

ANALYSIS

Specimen Configuration and Loading

Figure 1 shows the tapered laminate that was analyzed. The stacking sequence is $\{[0_7/(\pm45)]/_t$ $[(\pm45)_3]/[0/(\pm45)/0]\}_s$. The $(0_7/\pm45)$ ply group in the laminate of Fig.1 forms the belt area, and the $(0/\pm45/0)_s$ laminate in the center forms the core. The transition from the thick region at the left to the thin region at the right is achieved by dropping the group of $(\pm45)_3$ plies in three distinct steps, each 20-ply thicknesses apart. The shaded regions shown in Fig.1 are the resin pockets formed at the ends of the ±45 degree plies that are terminated. In similar laminates, delaminations have been observed at the interface indicated by the arrow in the layup above. Therefore, the delaminations are assumed to grow along the interface ABCD in Figure 1a. A typical delamination is shown in Fig. 1b. The delamination is assumed to form at point C, and grows into the tapered region (tip I) and into the thin region (tip H).

The tapered laminate was assumed to be made of S2/SP250 glass/epoxy and to be subjected to a uniform load at the thick end (X=0). Examination of the

5

results indicates that the displacements are uniform in the neighborhood of X=60h. Thus, the uniform load condition at X=0 is equivalent to a uniform displacement condition. A fixed grip condition was assumed at the thin end. The material properties used in the analysis are given in Table 1. The in-plane properties for a unidirectional ply (e.g; E_{11}, E_{22}, G_{12}, ν_{12}) are similar to those used in reference 7. The out-of-plane properties (G_{13}, ν_{13}, G_{23}, ν_{23}) were assumed to be identical to the in-plane properties, and E_{33} was assumed equal to E_{22}.

Finite Element Model

A 3-D finite element analysis of the laminate is desirable, but such analyses are complex. Simple 2-D models, which do not account for the free edges, usually provide insight that can be used in 3-D analyses. Thus, as a first step, 2-D plane-strain analyses were performed in this study. Furthermore, the stacking sequence considered here contains only 0 degree and ±45 degree plies. With the absence of the 90 degree plies, the interlaminar Poisson mismatch between plies that causes edge delaminations was not considered to be significant [5]. Therefore, a two dimensional finite-element analysis is expected to be reasonably accurate for this laminate.

A two dimensional finite element model was developed utilizing the symmetry of the laminate about the X-axis. The model had 7610 nodes and 2382 eight-noded, isoparametric, parabolic elements as shown in Fig. 2a. A refined mesh was used near plydrop points (B, E and F and C in Figure 1b) to capture the local influence of these geometric discontinuities and the corresponding stresses. The smallest element size used in the model was

equal to one-quarter of the ply thickness. These small elements were provided near the plydrops on line BC, at the transition point B from the thick region to the tapered region, and the transition point C from the tapered region to the thin region. The element size immediately below line BC varied in the Z-direction due to the change in the resin thickness from two to zero ply thicknesses in the three resin pockets. Collapsed eight-noded elements were used at locations E, F, and C in the resin pockets. Figure 2b shows local mesh detail at location E. A similar pattern was used at points F and C.

The nodes at the end of the thin region (at X = 180h in Figure 1a) of the laminate were constrained in both X- and Z- directions. A uniform tension per unit area, σ_o, (assuming a unit width in the Y-direction) was applied along the X=0 line of the model. Plane strain conditions were used in the analysis.

To facilitate modeling delaminations along ABCD, duplicate nodes were created in the model all along lines AB, BC, and CD. Multi-point constraints were imposed for the duplicate nodes. Different size delaminations were simulated by relaxing the multi-point constraints for the appropriate nodes along lines BC and CD. Note that two delaminations are assumed to maintain symmetry about the X-axis.

The material directions of plies in the laminate are oriented at an angle relative to the global coordinate system of the analysis. The material stress-strain relations for these plies were transformed to obtain the stress-strain relations in the global system. Appendix A presents the details of the transformations used.

7

Computation of Strain-Energy-Release Rate

The virtual crack closure technique (VCCT) was used to obtain the strain-energy-release rate components, mode I, and mode II, based on the local forces at and ahead of, and the relative displacements behind, the delamination tip. These two components were calculated using the following equations (see Fig.3).

$$G_I = - \frac{1}{2\Delta} \left[F_{ni} \left(v_k - v_{k'} \right) + F_{nj} \left(v_m - v_{m'} \right) \right] \qquad (1a)$$

$$G_{II} = - \frac{1}{2\Delta} \left[F_{ti} \left(u_k - u_{k'} \right) + F_{tj} \left(u_m - u_{m'} \right) \right] \qquad (1b)$$

where Δ is the element size, F_{ni} and F_{ti} are the normal (n) and tangential (t), forces, respectively, at node i, and $(v_k - v_{k'})$ and $(u_k - u_{k'})$ are the relative opening and sliding displacements, respectively, at node k (see Fig.3). Forces at node j and relative displacements at nodes m and m' are defined similarly. Equations 1 are similar to those given in references 8 and 9. The total strain-energy-release rate, G, at the delamination tip was calculated as

$$G = G_I + G_{II} \qquad (2)$$

The mode III component of G was identically zero because plane strain conditions were assumed in the analyses.

Alternatively, the global energy change of the laminate due to delamination growth can also be used to calculate the total strain-energy-release rate, G. The strain energy of the laminate, U, can be conveniently computed as $U = 1/2(\Sigma f_i u_i)$ where f_i and u_i are the nodal forces and corresponding nodal displacements, respectively, for all nodes i on the line X=0 in Figure 1a. The strain-energy-release rate for successive delamination growth was calculated as

$$G = \frac{dW}{dA} - \frac{dU}{dA} \qquad (3a)$$

where dW/dA and dU/dA are the rate of change of work and strain energy, respectively, with change in delamination area. In the finite-element analysis, Equation (3a) can be computed as

$$G = (U_{x+dx} - U_x)/dx \qquad (3b)$$

where U_{x+dx} and U_x are the strain energies for delamination lengths x+dx and dx, respectively. The value of G thus calculated is considered to be the strain-energy-release rate at (x+ dx/2), which is located at the center of the interval.

RESULTS AND DISCUSSION

First, the interlaminar stress distributions along the interface ABCD are presented. Next, the strain-energy-release rate variations for various size delaminations assumed along the interface line ABCD are shown. Finally,

the peak values of the total strain-energy-release rate and the mode I component values are presented and their significance discussed.

Interlaminar Stresses

Figure 4 shows the normalized interlaminar normal stress, (σ_n/σ_o), along lines AB, BC, and CD in the laminate. Stresses were calculated in the local coordinate system, normal to the interface ABCD. The interlaminar normal stress shows peaks near the points of geometric and material discontinuity i.e. at points B, E, F, and C. The largest tensile value of the σ_n distribution occurred at the transition point C. At the plydrops, points B, E, F, the stresses changed from a high compressive value immediately to the left of the plydrop to a high tensile value immediately to the right of plydrop. The variation of normalized interlaminar shear stress, (τ_{nt}/σ_o), along the same interfaces AB, BC, and CD is shown in Figure 5. The shear stress also shows peaks at points B, E, F and C.

These sudden changes in the normal and shear stress distributions at points B, E, F, and C are not unexpected. At these points, the material stiffness is different in different directions (see Fig. 6). Therefore, at points B, E, F, and C, stress singularities probably exist [10].

In order to investigate if this is true, a two-dimensional finite-element analysis of a homogeneous tapered laminate was performed with the same model as in Fig. 2. The tapered laminate was assumed to be of an isotropic material. The normalized interlaminar normal stress (σ_n/σ_o) distribution along the line ABCD is presented in Fig. 7. At points E and F, the stiffness is same in different directions irrespective of how these points are approached. Thus, no sudden changes in stress distribution exist

at these points. The normals to lines AB and BC at point B have different directions. Similarly, normals to lines BC and CD are different at point C. Thus, except for very small discontinuities at these points, the stress distribution all along ABCD is smooth. This confirms that the sharp changes in stresses observed in Figures 4 and 5 are solely due to material discontinuities at the points B, E, F, and C.

Strain-Energy-Release Rate Analysis

Delamination growth in a laminated composite structure may be predicted from the mode I, and mode II components of the strain-energy release rate under static loading and from the total strain-energy-release rate for fatigue loading [5,7]. The computation and the use of the strain-energy-release rate in delamination prediction for the tapered laminate are discussed below.

As seen in Figure 4, point C has the highest value of interlaminar normal stress, σ_n, compared to any other location on the interface line ABCD. Therefore, the delamination was assumed to initiate at this point. Delamination lengths a and b (see Fig. 1b) were assumed within the tapered region along CB and in the thin laminate along CD, respectively. The strain-energy-release rate values G, G_I, and G_{II} were computed at each delamination tip using the finite element analysis and Equations 1-3 for various values of a and b.

The total strain-energy-release rates were calculated using two different methods; VCCT (equation 2) and from global energy change (equation 3). These G values normalized by N_x^2/h, (where N_x is defined as the product

of uniform tension stress σ_o and half the laminate depth at $X = 0$, and h is the ply thickness), are plotted for comparison in Figure 8. For this case, no delamination was assumed along the taper, CB, (i.e. a=0) and the values of G were obtained for various values of delamination lengths, b, along CD in the thin region of the laminate. Excellent agreement between the G values computed by the two methods was obtained. Similar agreement was found for all the cases studied. The G values obtained by using equation 3 are presented in this paper because more data points were available for this computation and values of the individual modes, G_I and G_{II}, were taken from the VCCT calculation.

Figure 9 presents a composite of G distributions for delamination growth in the thin and thick regions. In the right hand portion of the figure, the G values for the delamination tip at "H" were plotted against b/h for a fixed value of a/h. Similarly, the left hand portion of Figure 9 presents the G values for the delamination tip "I" plotted against a/h for a fixed value of b/h.

Referring to the delamination tip at "H" on the right side of Figure 9 (where a/h is held constant and b/h varies), the G initially increases rapidly with b/h as the delamination grows into the thin laminate along line CD. For a/h= 0, 6, and 12, the G attains a peak value and drops slightly with further delamination growth. This drop decreases with increasing a/h and does not occur for a/h= 20 and 24 in the range of b/h considered. These values of G are given in Table 2.

In a complementary situation shown on the left side of Figure 9, the G values at the delamination tip I were plotted against a/h for various values of b/h. The total strain-energy-release rate increases initially, and then is relatively constant, or drops slightly, before approaching the plydrop.

In the proximity of the dropped plies, however, G values increase rapidly and attain peak values at the plydrops (a=20h and 40h). These G values are given in Table 3.

The results of Figure 9 suggest that a delamination initiating at point C will grow in an unstable manner simultaneously along the tapered interface CB as well as in the thin laminate along CD. This can be explained as follows. Consider a small delamination initiating at point C in Fig. 9. If G for the left and right delamination tips control growth along the thin and tapered regions, respectively, then delaminations would arrest after they had grown to the peak values. However, growth of one delamination tip will increase the G for the other tip, causing growth in that direction also. Hence, as soon as a stable situation occurs on one delamination tip, it will increase the G for the other tip causing further growth. Hence, as the peaks in the G values on the left and right sides of Figure 9 increase monotonically with increasing a/h and b/h, a delamination initiating at point C will grow unstably in both directions simultaneously.

As discussed above, the values of G shown in Fig. 9 reached peak values for delamination growth in either direction. For delamination growth along the thin side CD, the plots of G for delamination tip "H" vs. b/h are similar to those obtained for edge delamination, where G is initially zero at b/h=0 and increases to a plateau at some distance, usually b/h≈ 2 to 3 [5-7]. The distance at which G reaches a plateau for the edge case may vary with the interface analyzed [5]. Similarly, the distance at which G at tip "H" vs. b/h reaches a peak varies with a/h. The value of b/h to reach this peak, however, is of little consequence since it is assumed that the plateau, or peak value of G governs the delamination onset at the edge or, in this case, at the initial point of the taper [5]. The peak values of G

on the right side in Figure 9 are plotted on the right side of Figure 10 as a function of the corresponding a/h. Similarly, the peak G values on the left side in Figure 9, occurring near point C, are plotted on the left side of Figure 10 as a function of the corresponding b/h. The numerical values are included in Table 4. The peak G values at a/h=0 (for b/h=4.5) and at b/h=0 (for a/h=5.75) are nearly equal and may be hypothesized as the critical value for the onset of a delamination at point C under fatigue loading. Delamination in the tapered laminate can be predicted by comparing this value to the threshold for delamination onset [6].

If the delamination initiates at point C under static tension loading, its growth will be governed by a mixed-mode criterion [5] because both the mode I and mode II components of G are present due to the tapered configuration. Figure 11 shows the percentages of mode I and mode II at delamination tip H in the thin laminate corresponding to a value of a=24h. Table 5 summarize results for several values of a/h. The mode I component is predominant for all values of b/h ≤ 18.

In contrast, as shown in Figure 12 and Table 6, the G components at delamination tip I in the tapered region CB initially consists of a large mode I component but at a/h=18 the mode I component is only 50 percent of the total and continues to decrease with increasing a/h. Near the plydrops, G_I drops suddenly, but then increases. Overall, G_I decreases with increasing a/h, and G_{II} increases with increasing, a/h. The value of G_I is approximately zero (i.e. G becomes 100 percent mode II) at a/h= 54. This distance depends on the initial delamination length, b/h, in the thin laminate.

The mode I component of G is predominant for a small delamination initiating at point C (Fig.1) and growing either along CD (Fig.11) or along

CB (Fig.12). The corresponding peak G_I values for various a/h and b/h ratios are shown in Table 7 and are plotted in Fig. 13. This figure is constructed in similar manner to Fig.10. The peak G_I values at a/h=0 for growth into the thin region or at b/h=0 for growth into the tapered region may be compared to G_{IC} for the composite to predict delamination onset under static tension loading[5].

CONCLUDING REMARKS

A tapered composite laminate subjected to tension load was analyzed using the finite element method. The stacking sequence of the laminate was assumed to be $\{[0_7/(\pm45)]/_\uparrow$ $[(\pm45)_3]/[0/(\pm45)/0]\}_s$. The group of $(\pm45)_3$ plies was dropped in three distinct steps, each 20 ply-thicknesses apart, thus forming a taper angle of 5.71 degrees. Neat resin pockets are assumed at the ends of ±45 degree plies that were terminated. The material of the laminate was assumed to be S2/SP250 glass/epoxy.

A two-dimensional plane strain analysis was performed to determine stress distributions in the laminate without a delamination. The interlaminar normal stress and interlaminar shear stress distribution along the tapered interface, indicated by an arrow in the above stacking sequence, were calculated. Then delaminations were assumed to initiate at the point of intersection of the tapered interface and the thin region of the laminate. Delamination growth in the finite element model was simulated along the taper and into the thin region. The total strain-energy-release rate, G, and the mode I, and mode II components, G_I and G_{II}, were computed at the delamination tip using the virtual crack closure technique (VCCT).

15

Alternatively, G was obtained from a global energy balance. Based on the analysis performed here, the following conclusions were reached:

1) Steep gradients of interlaminar normal and shear stress exist at the points of material and geometric discontinuities created by the internal plydrops. The largest value of interlaminar normal stress appears to occur at the intersection of the tapered interface and the thin region of the laminate. This is probably the site where a delamination would initiate.

2) The strain-energy-release rate, G, was calculated for a delamination initiating at a point, located at the intersection of the taper and the thin laminate, and lying on the interface indicated by the arrow in the layup. The G values increase continually as the delamination grows into the thin laminate portion or along the taper. This indicates that a delamination initiating at the end of the taper will grow unstably along the taper and the thin laminate simultaneously.

3) The strain-energy-release rate for a delamination growing a short distance into the thin laminate consists predominantly of mode I (opening) component.

4) For a delamination growing along the tapered region, the strain-energy-release rate was initially all mode I but decreased with increasing delamination size until eventually it was all mode II.

These results may help understand the delamination behavior in the tapered laminates and may be useful in predicting the onset and growth of the delamination under static and fatigue loading.

REFERENCES

[1] Adams, D. F., Ramkumar, R. L., Walrath, D.E., "Analysis of Porous Laminates in the Presence of Ply Drop-offs and Fastener holes," Northrop Technical Report 84-113, May 1984, One Northrop Avenue, Hawthorne, CA 90250 and University of Wyoming, Mechanical Engineering Department, Laramie, WY 82071.

[2] Cannon, R. K., "The Effect of Ply Dropoffs on the Tensile Behavior of Graphite/epoxy Laminates," TELAC Report 87-12, May 1987, M.I.T., Cambridge, MA. 02139.

[3] Kemp, B. L., Johnson, E. R., "Response and Failure Analysis of a Graphite-Epoxy Laminate containing Terminating Internal Plies," Paper No. AIAA-85-0608, Proceedings of the AIAA, ASME, ASCE, AHS, 26th Structures, Structural Dynamics and Materials Conference, Orlando, Florida, 1985, pp 13-24.

[4] O'Brien, T.K., Murri, G.B., and Salpekar, S.A., "Interlaminar Shear Fracture Toughness and Fatigue Thresholds for Composite Materials," NASA TM 89157, August, 1987, Presented at the 2nd ASTM symposium on <u>Composite Materials: Fatigue and Fracture</u>, Cincinnati, OH, April, 1987.

[5] O'Brien, T. K., "Mixed-mode Strain-Energy-Release Rate Effects on Edge Delamination of Composites," ASTM STP 836, <u>Effects of Defects in Composite Materials</u>, American Society for Testing and Materials, Philadelphia, PA, 1982, p.125.

[6] O'Brien, T. K., "Towards a Damage Tolerance Philosophy for Composite Materials and Structures," Presented at the 9th ASTM Symposium on Composite Materials: Testing and Design, Reno, Nevada, April 27-29, 1988, (NASA TM 100548, May, 1988).

[7] Chan, W. S., Rogers, C., Aker, S., "Improvement of Edge Delamination Strength of Composite Laminates Using Adhesive Layers," <u>Composite Materials :Testing and Design</u>, ASTM STP 893, 1986, p.266.

[8] Rybicki, E. F., and Kanninen, M. F., "A Finite Element Calculation of Stress-Intensity Factors by a Modified Crack-Closure Integral," <u>Engineering Fracture Mechanics,</u> Vol. 9, 1977, pp. 931-938.

[9] Raju, I. S., "Calculation of strain-energy-release rates with Higher Order and Singular Finite Elements."   Engineering Fracture Mechanics, vol.28, 1987, pp. 251-274.

[10] Erdogan, F., Stress distribution in bonded dissimilar materials with cracks, J. appl. Mech. 32, Series E, 403(1965).

Appendix A

Transformation of Stiffness Coefficients

The stress-strain relations for each lamina were transformed from the material coordinate system 1,2,3 (Fig. 14) to the global system XYZ using the following procedure. The 3-D stress-strain relation for a ply in the material coordinate system is

$$\{\sigma\}_{123} = [C] \{\epsilon\}_{123} \qquad (A1)$$

where $\{\sigma\}_{123} = \{\sigma_{11} \quad \sigma_{22} \quad \sigma_{33} \quad \sigma_{12} \quad \sigma_{23} \quad \sigma_{13}\};$

$$\{\epsilon\}_{123} = \{\epsilon_{11} \quad \epsilon_{22} \quad \epsilon_{33} \quad \epsilon_{12} \quad \epsilon_{23} \quad \epsilon_{13}\};$$

and $[C]_{6x6}$ is a matrix that can be determined from elastic constants. Following similar notations, the stress-strain relations for a lamina in the global system can be written as

$$\{\sigma\}_{XYZ} = [C]' \{\epsilon\}_{XYZ} \qquad (A2)$$

The matrix $[C]'$ is obtained from matrix $[C]$ by rotating the material system 1,2,3 (Fig. 14) to the global coordinate system XYZ through two rotations; a rotation (θ) about the Z (or 3) axis, and then by a rotation (ϕ) about the Y (or Y') axis. The transformed stiffness coefficient matrix, $[C]'$, is obtained from the material stiffness coefficient matrix, $[C]$ as

$$[C]'_{6x6} = [T_\phi]_{6x6} [T_\theta]_{6x6} [C]_{6x6} [T_\theta]^T_{6x6} [T_\phi]^T_{6x6} \qquad (A3)$$

where $[T_\theta]$ and $[T_\phi]$ are defined in terms of the appropriate angle as

$$[T_\theta] = \begin{bmatrix} \cos^2\theta & \sin^2\theta & 0 & 2*\cos\theta*\sin\theta & 0 & 0 \\ \sin^2\theta & \cos^2\theta & 0 & -2*\cos\theta*\sin\theta & 0 & 0 \\ 0 & 0 & 1.0 & 0 & 0 & 0 \\ -\cos\theta*\sin\theta & \cos\theta*\sin\theta & 0 & \cos^2\theta - \sin^2\theta & 0 & 0 \\ 0 & 0 & 0 & 0 & \cos\theta & -\sin\theta \\ 0 & 0 & 0 & 0 & \sin\theta & \cos\theta \end{bmatrix}$$

and

$$[T_\phi] = \begin{bmatrix} \cos^2\phi & 0 & \sin^2\phi & 0 & 0 & 2*\cos\phi*\sin\phi \\ 0 & 1.0 & 0 & 0 & 0 & 0 \\ \sin^2\phi & 0 & \cos^2\phi & 0 & 0 & -2*\cos\phi*\sin\phi \\ 0 & 0 & 0 & \cos\phi & \sin\phi & 0 \\ 0 & 0 & 0 & -\sin\phi & \cos\phi & 0 \\ -\cos\phi*\sin\phi & 0 & \cos\phi*\sin\phi & 0 & 0 & \cos^2\phi - \sin^2\phi \end{bmatrix}$$

The superscript T to a matrix in equation (A3) denotes the transpose of the matrix. Furthermore, the plane strain conditions require that $\epsilon_{YY} = \epsilon_{XY} = \epsilon_{YZ} =$

0. Incorporating these conditions in (A2) yields the stress-strain relations for plane strain as

$$\{\sigma\}_{XZ} = [C]'_{XZ} \{\epsilon\}_{XZ} \qquad (A4)$$

where $\{\sigma\}_{XZ} = \{\sigma_{XX} \quad \sigma_{ZZ} \quad \sigma_{XZ}\}$; $\{\epsilon\}_{XZ} = \{\epsilon_{XX} \quad \epsilon_{ZZ} \quad \epsilon_{XZ}\}$.

and $[C]'_{XZ}$ is obtained from the global $[C]'$ matrix as,

$$[C]'_{XZ} = \begin{bmatrix} c'_{11} & c'_{13} & c'_{16} \\ c'_{31} & c'_{33} & c'_{36} \\ c'_{61} & c'_{63} & c'_{66} \end{bmatrix} \qquad (A5)$$

TABLE 1:   MATERIAL PROPERTIES USED IN THE ANALYSES

S2/SP250 GLASS/EPOXY: RESIN:

E_{11} $= 7.30$ MSI $E = 0.59$ MSI

E_{22}, E_{33} $= 2.10$ MSI $G = 0.224$ MSI

G_{12}, G_{13}, G_{23} $= 0.88$ MSI $\nu = 0.33$

ν_{12}, ν_{13}, ν_{23} $= 0.275$

TABLE 2: TOTAL STRAIN-ENERGY-RELEASE RATE AT DELAMINATION TIP 'H'

IN THE THIN LAMINATE

$Gh/N_x^2 *10^{12} \frac{in.^2}{lb.}$

b/h	a/h=0	a/h=6	a/h=12	a/h=20	a/h=24
.43	10.57	110.00	171.00	230.71	287.86
.90	17.50	113.58	178.67	242.83	302.42
1.50	24.17	115.75	185.08	254.08	316.17
2.10	28.42	116.08	189.00	262.42	326.67
3.00	31.79	116.21	194.63	275.33	343.54
4.20	32.79	114.33	199.00	288.83	362.08
5.40	31.67	111.63	201.42	299.92	378.25
6.90	29.25	107.78	203.00	311.81	396.61
8.70	26.08	102.81	202.83	322.64	414.75
10.80	22.85	96.98	200.69	331.40	431.29
15.00	18.15	86.74	194.06	341.78	455.43
21.00	13.59	73.30	178.81	339.28	465.62
30.00	12.20	64.98	166.61	336.18	474.39

TABLE 3:   TOTAL STRAIN-ENERGY-RELEASE RATE AT DELAMINATION TIP 'I'

ALONG THE TAPER

$Gh/N_x^2 *10^{12} \frac{in.^2}{lb.}$

a/h	b/h=0	b/h=6	b/h=12	b/h=24
.75	19.40	93.10	173.00	260.90
2.75	42.23	130.46	207.04	333.14
5.75	47.82	131.12	224.82	400.60
7.50	45.60	126.15	224.90	424.00
9.00	43.50	121.25	222.48	437.50
11.00	40.93	113.55	214.75	445.25
13.00	38.58	104.63	202.65	440.25
15.00	37.05	95.13	186.20	421.25
17.00	42.55	94.55	177.88	401.50
18.50	70.30	128.40	214.25	439.50
19.13	115.40	183.40	276.20	510.00
19.38	113.20	181.40	273.40	502.00
19.63	132.60	205.40	300.20	530.00
19.88	160.40	238.60	336.80	570.00
20.13	275.20	413.40	590.00	1004.00
20.38	298.20	418.20	577.00	970.00
20.63	288.00	397.20	544.40	916.00

TABLE 3 (contd.)

a/h	$Gh/N_x^2 *10^{12} \ \frac{in.^2}{lb.}$			
	b/h=0	b/h=6	b/h=12	b/h=24
21.00	280.10	383.50	523.70	882.00
22.13		336.20	471.11	822.86
24.50		256.55	383.63	729.75
27.00		207.35	323.40	657.03
29.00		184.30	291.20	611.98
31.00		167.33	264.48	569.05
34.00		148.30	228.23	497.18
37.75			241.60	469.31
39.63			340.20	578.00
39.88			380.20	629.40
40.25			636.40	1082.60
40.75			624.50	1011.20
42.00			581.33	935.78
44.50			483.47	808.02
48.00				671.81
51.00				573.73
53.00				512.15

TABLE 4 :   PEAK VALUES OF TOTAL STRAIN-ENERGY-RELEASE RATE

DELAMINATION TIP	a/h	b/h	$\underline{\text{PEAK } G{*}h{*}10^{12}} \quad \underline{\text{in}^2}$
			$N_X^2 \qquad\qquad \text{lb.}$

H	0.0	4.5	32.5
H	6.0	3.0	116.5
H	12.0	7.0	204.0
H	20.0	14.5	340.0

I	5.75	0.0	47.5
I	3.00	6.0	130.0
I	6.00	12.0	220.0
I	11.00	24.0	450.0

TABLE 5a: PERCENTAGE OF G_I/G AT DELAMINATION TIP 'H'

IN THE THIN LAMINATE

- -

$$\frac{G_I}{G} \times 100$$

b/h	a/h=0	a/h=6	a/h=12	a/h=20	a/h=24
1.20	99.05	98.33	97.69	96.92	95.74
1.80	97.69	99.66	99.19	98.64	97.73
3.60	94.57	99.88	100.00	100.00	99.88
4.80	92.16	98.72	99.50	99.86	100.00
7.80	86.53	95.25	97.07	98.00	98.91
18.00	73.01	87.43	91.40	93.17	94.89

- -

TABLE 5b: PERCENTAGE OF G_{II}/G AT DELAMINATION TIP 'H'

IN THE THIN LAMINATE

- -

$$\frac{G_{II}}{G} \times 100$$

b/h	a/h=0	a/h=6	a/h=12	a/h=20	a/h=24
1.20	0.95	1.67	2.31	3.08	4.26
1.80	2.31	0.34	0.81	1.36	2.27
3.60	5.43	0.12	0.00	0.00	0.12
4.80	7.84	1.28	0.50	0.14	0.00
7.80	13.47	4.75	2.93	2.00	1.09
18.00	26.99	12.57	8.60	6.83	5.11

TABLE 6a: PERCENTAGE OF G_I/G AT DELAMINATION TIP 'I'

ALONG THE TAPER

- -

$$\frac{G_I}{G} \times 100$$

a/h	b/h=0	b/h=6	b/h=12	b/h=24
.50	88.46	99.25	99.38	99.20
1.00	86.15	97.13	97.80	97.80
4.50	71.85	83.68	87.53	89.70
7.00	56.77	73.17	79.66	83.80
10.00	39.98	62.67	72.46	79.10
12.00	29.09	55.29	67.48	76.10
14.00	18.82	47.35	62.14	73.00
16.00	10.09	37.74	55.11	68.90
19.25	11.61	26.88	40.54	56.00
19.50	13.27	27.33	40.01	54.80
19.75	14.27	26.50	37.67	51.30
20.00	13.95	25.09	35.10	47.50
20.25	6.61	18.69	30.59	45.80
20.50	2.00	11.00	22.26	38.60
20.75	1.01	8.70	19.53	36.20
21.25	.54	7.36	17.91	34.70

TABLE 6a (contd.)

$$\frac{G_I}{G} \times 100$$

a/h	b/h=0	b/h=6	b/h=12	b/h=24
23.00		9.59	21.51	39.30
26.00		10.33	23.84	43.00
28.00		8.67	22.55	42.80
30.00		6.36	20.17	41.70
32.00		3.85	17.02	39.80
36.00		.09	8.67	32.60
39.50			9.61	26.80
39.75			10.58	26.10
40.00			13.11	27.70
40.50			6.28	21.20
41.00			3.36	16.60
43.00			2.75	16.30
46.00			1.76	16.00
50.00				10.20
52.00				5.70
54.00				1.10

TABLE 6b: PERCENTAGE OF G_{II}/G AT DELAMINATION TIP 'I'

ALONG THE TAPER

$$\frac{G_{II}}{G} \times 100$$

a/h	b/h=0	b/h=6	b/h=12	b/h=24
.50	11.54	.75	.62	.80
1.00	13.85	2.87	2.20	2.20
4.50	28.15	16.32	12.47	10.30
7.00	43.23	26.83	20.34	16.20
10.00	60.02	37.33	27.54	20.90
12.00	70.91	44.71	32.52	23.90
14.00	81.18	52.65	37.86	27.00
16.00	89.91	62.26	44.89	31.10
19.25	88.39	73.12	59.46	44.00
19.50	86.73	72.67	59.99	45.20
19.75	85.73	73.50	62.33	48.70
20.00	86.05	74.91	64.90	52.50
20.25	93.39	81.31	69.41	54.20
20.50	98.00	89.00	77.74	61.40
20.75	98.99	91.30	80.47	63.80
21.25	99.46	92.64	82.09	65.30

TABLE 6b (contd.)

$$\frac{G_{II}}{G} \times 100$$

a/h	b/h=0	b/h=6	b/h=12	b/h=24
23.00		90.41	78.49	60.70
26.00		89.67	76.16	57.00
28.00		91.33	77.45	57.20
30.00		93.64	79.83	58.30
32.00		96.15	82.98	60.20
36.00		99.91	91.33	67.40
39.50			90.39	73.20
39.75			89.42	73.90
40.00			86.89	72.30
40.50			93.72	78.80
41.00			96.64	83.40
43.00			97.25	83.70
46.00			98.24	84.00
50.00				89.80
52.00				94.30
54.00				98.90

TABLE 7:   PEAK VALUES OF mode I STRAIN-ENERGY-RELEASE RATE

DELAMINATION TIP	a/h	b/h	$\dfrac{G_I h}{N_x^2} * 10^{12}$ in.^{2}/lb.
H	0.0	3.60	30.12
H	6.0	1.80	115.67
H	12.0	4.80	198.68
H	20.0	7.80	309.81
I	4.5	0.0	35.02
I	4.5	6.0	111.75
I	4.5	12.0	194.11
I	7.0	24.0	345.76

33

Resin pocket

$(\pm45)_3$

A

B E F C $(O_7/\pm45)$ Belt

D

$\angle(O/\pm45/O)_s$ Core

σ_O

Z

X $\oplus$

60 h

20 h

60 h

60 h

Thin region

Tapered region

Laminate: $[O_7/\pm45/\wedge(\pm45)_3/O/\pm45/O]_s$

h = ply thickness
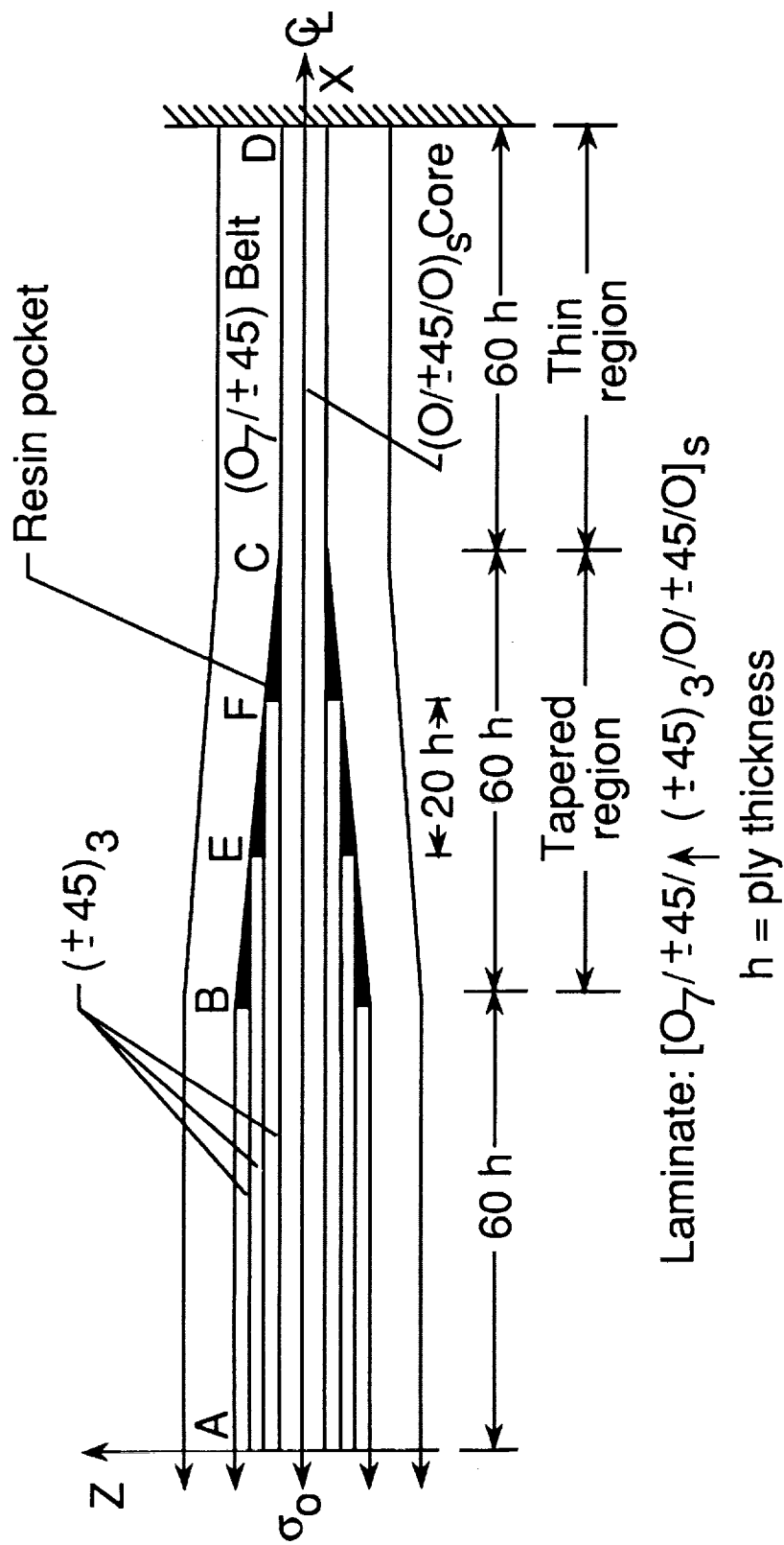
Fig. 1(a): Tapered laminate configuration and loading
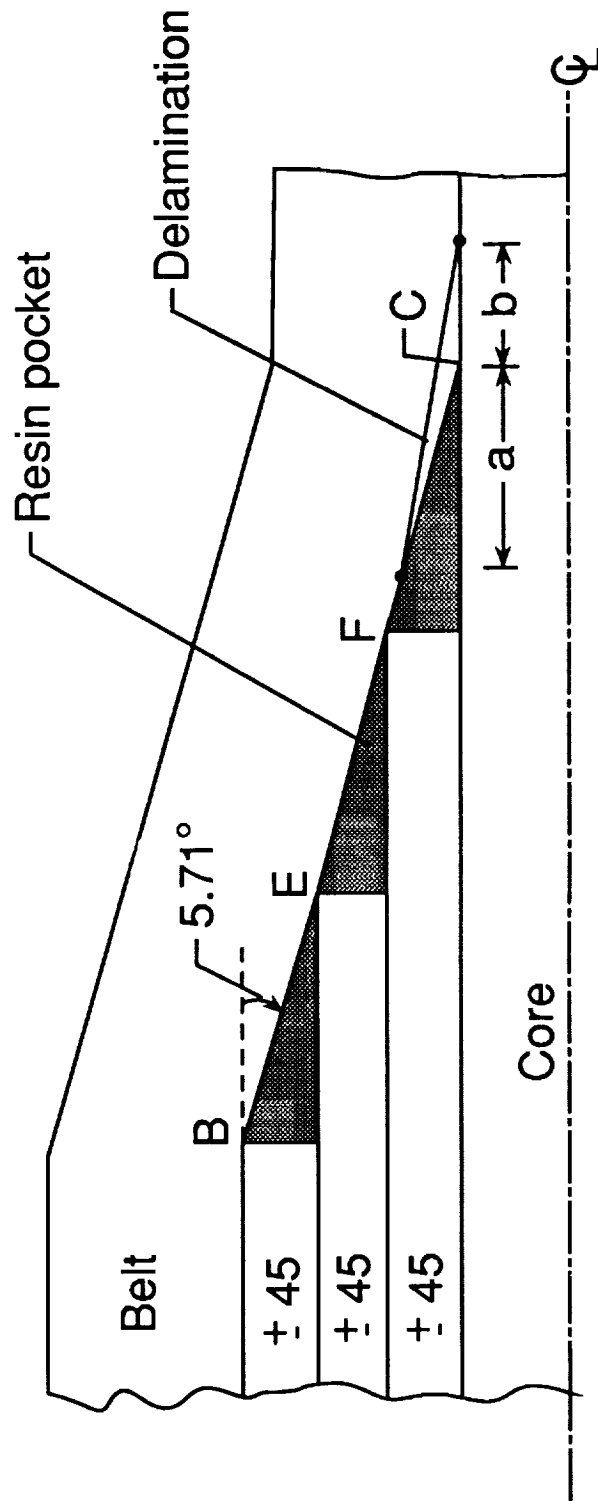
Fig. 1(b): Typical delamination
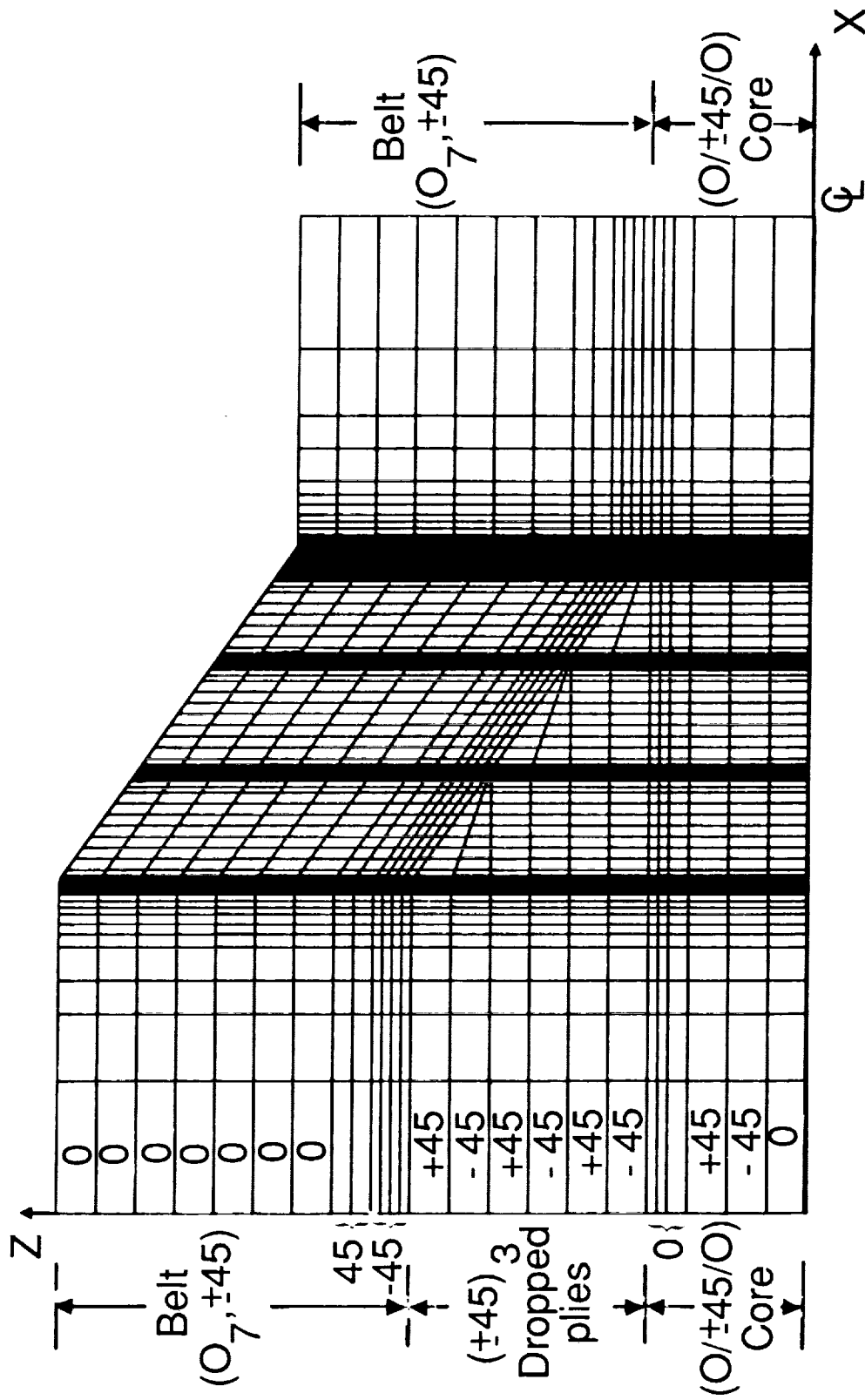
Fig. 2(a): Finite-element model of the tapered laminate
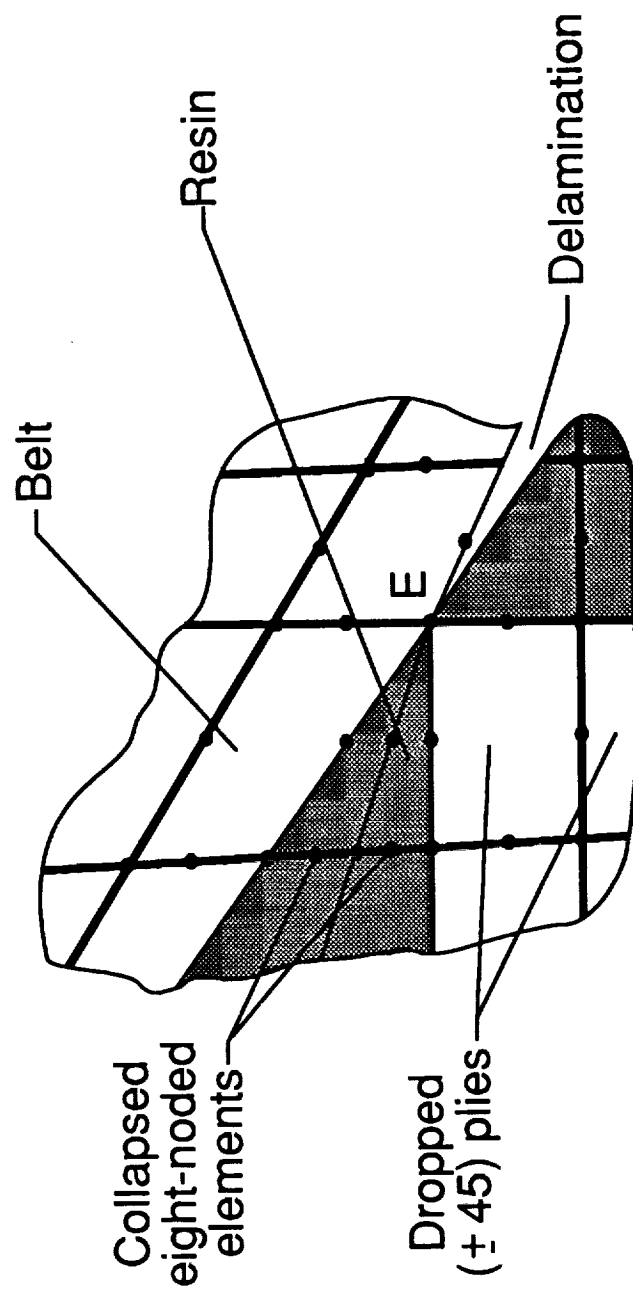
Fig. 2(b) : Mesh detail showing delamination tip at point E
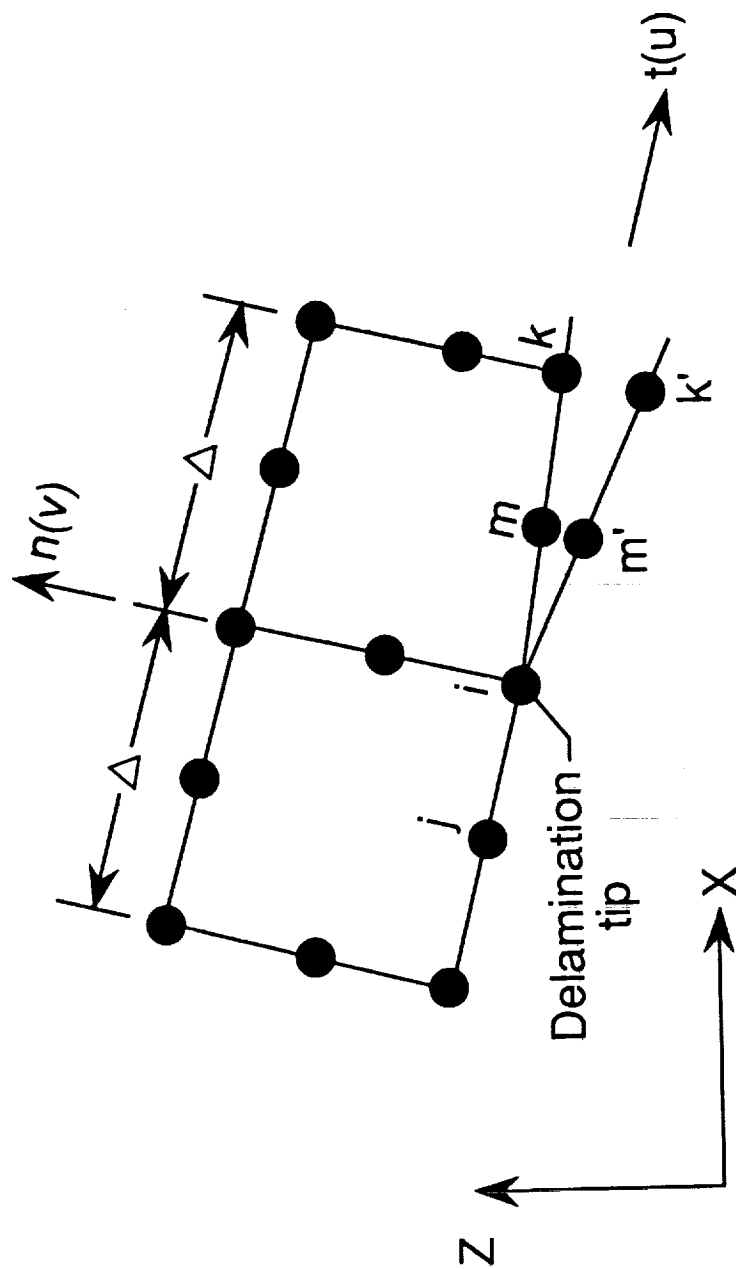
Fig. 3: Finite-element idealization near a delamination tip for calculating G using VCCT
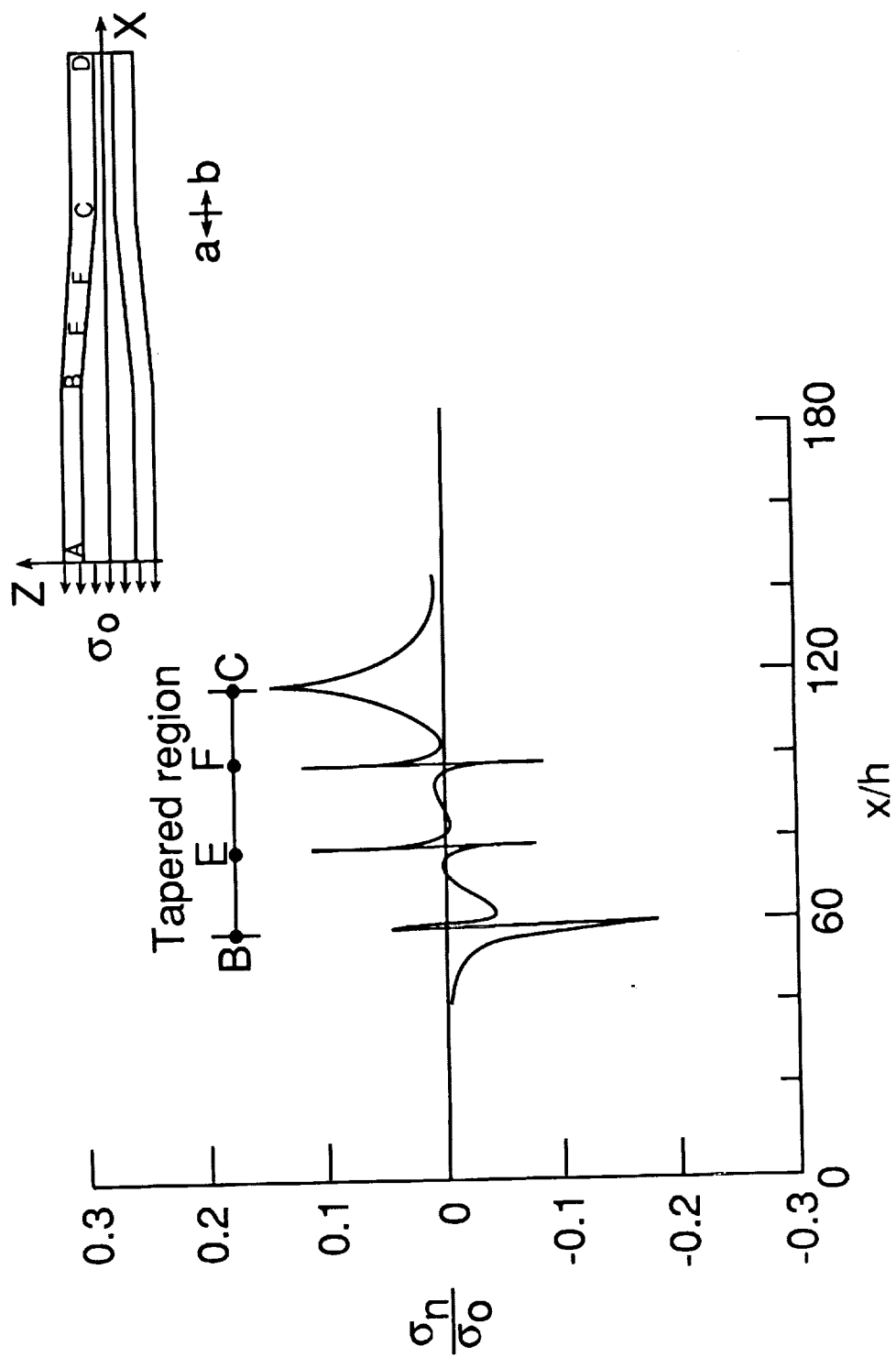
Fig. 4: Normalized interlaminar normal stress distribution along
the tapered interface BEFC
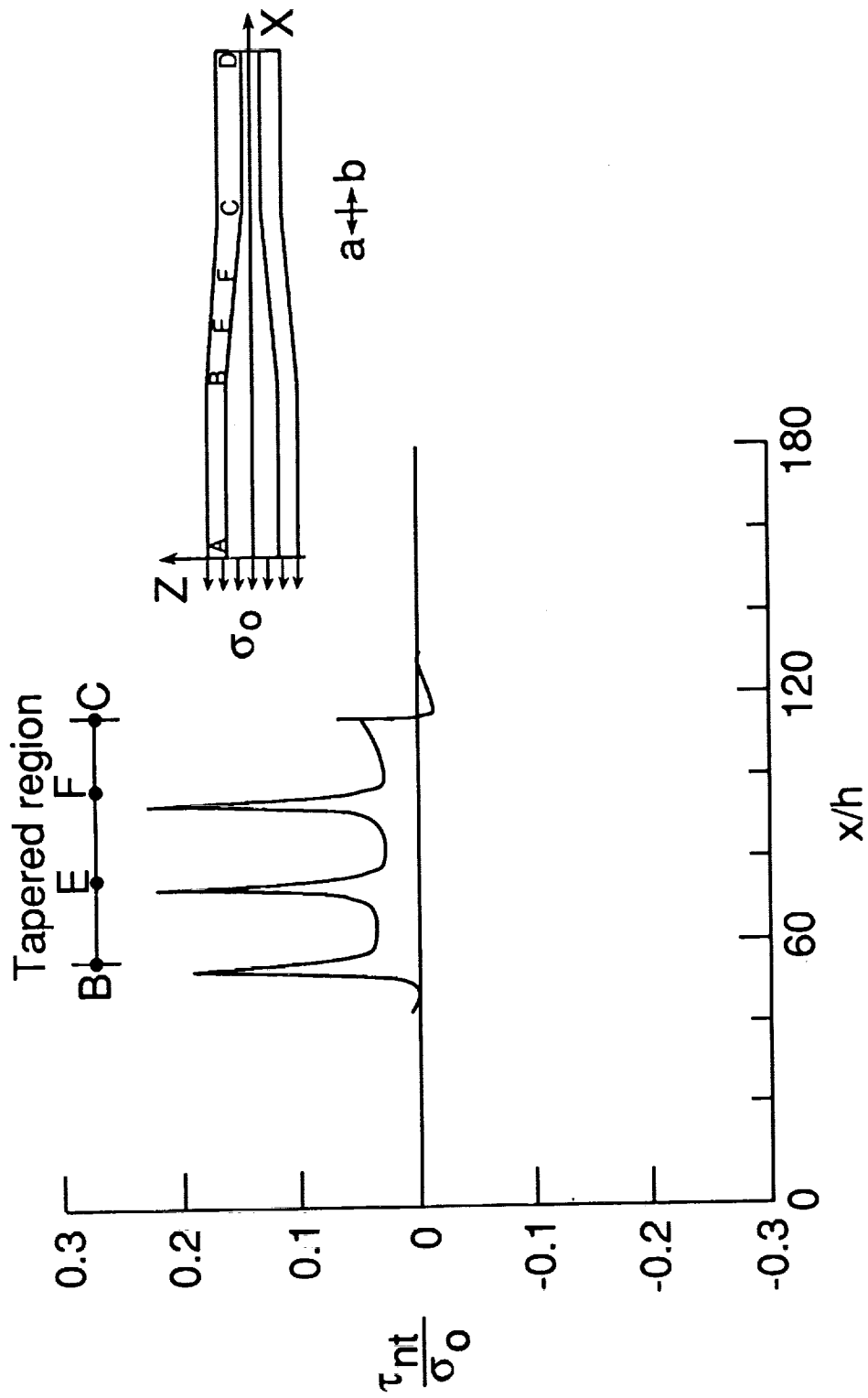
Fig. 5: Normalized interlaminar shear stress distribution along
tapered interface BEFC

Detail at point B

Detail at points E, F

Detail at point C
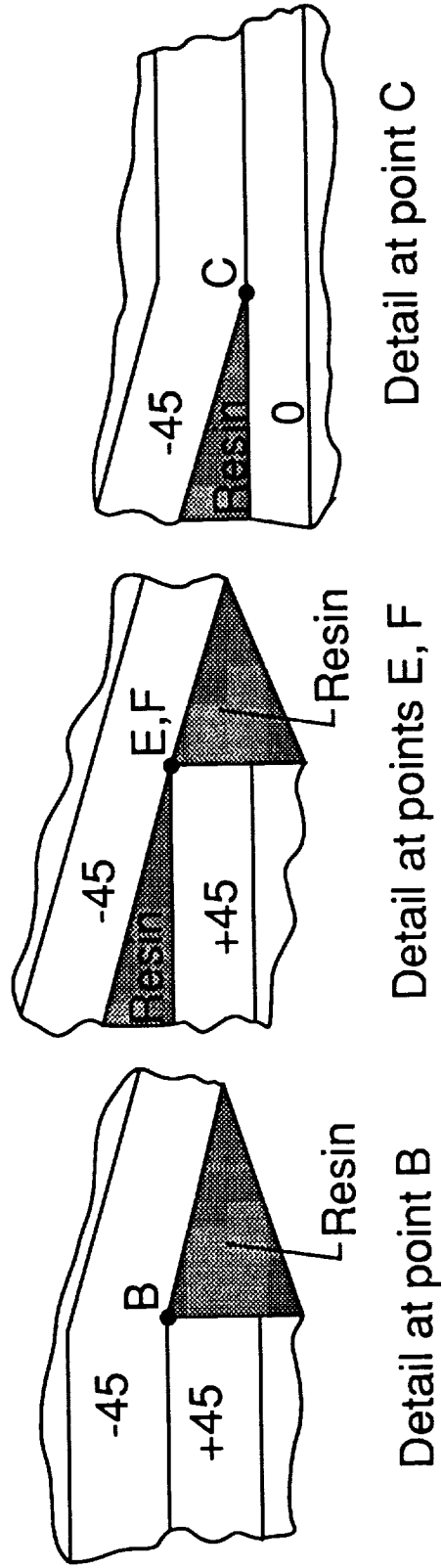
Fig. 6: Details of geometric and material discontinuities along

interface ABCD

41
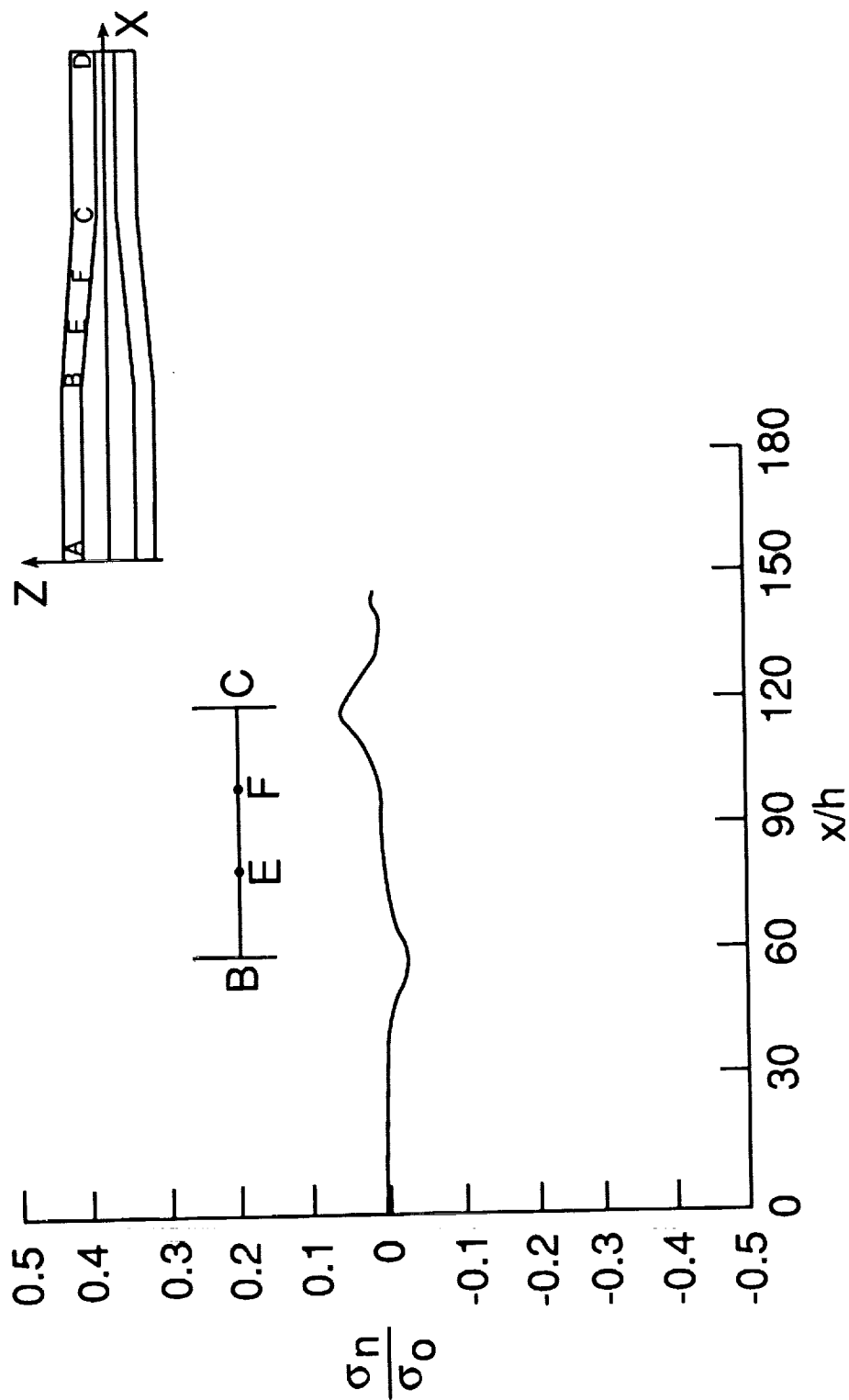
Fig. 7: Normalized interlaminar stress distribution along interface

ABCD in the tapered isotropic (resin) laminate

42
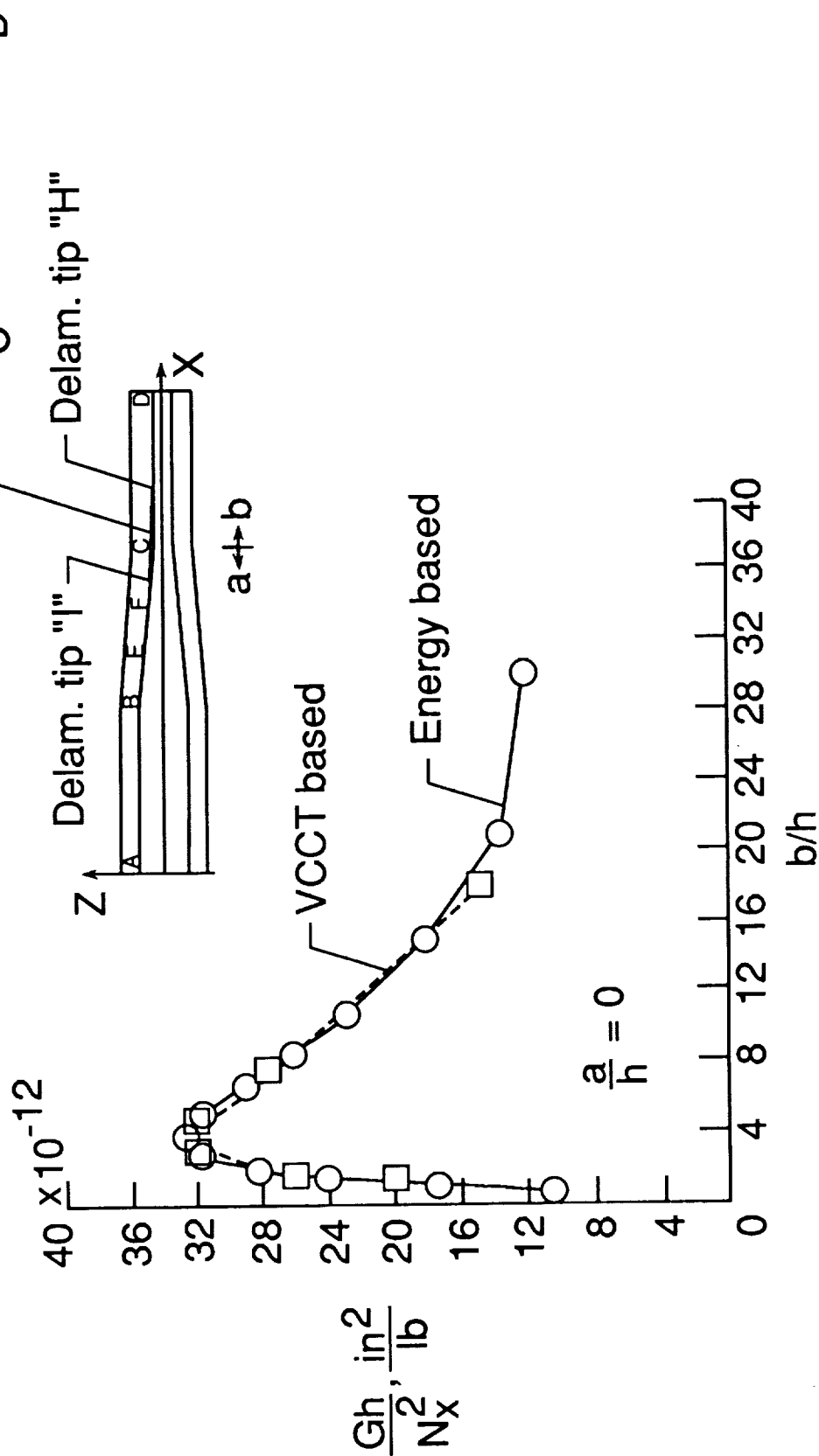
Fig. 8: Normalized total strain-energy-release rate at delamination tip H along interface CD
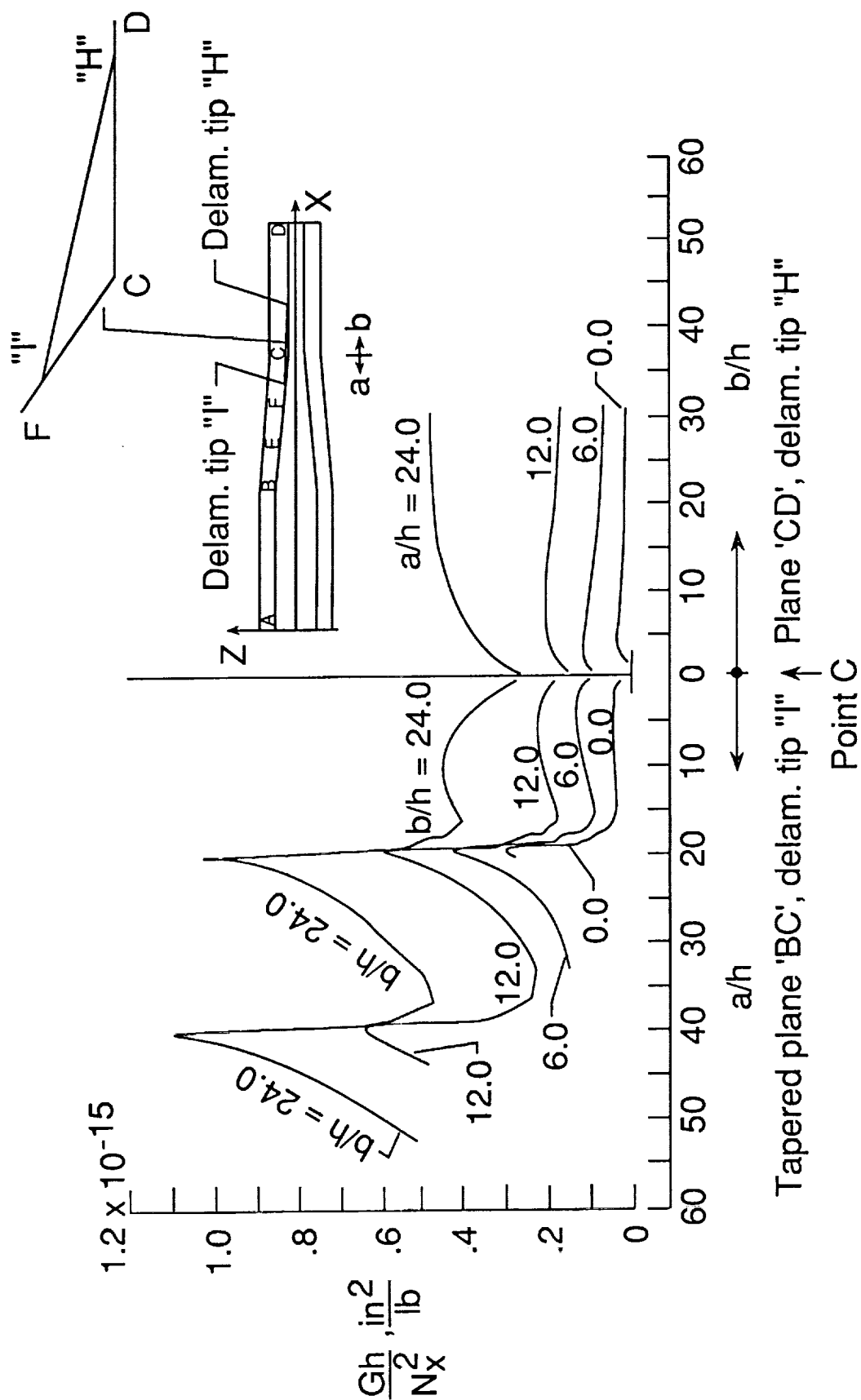
Fig. 9: Normalized total strain-energy-release rate at delamination
tip I along interface CB and tip H along interface CD
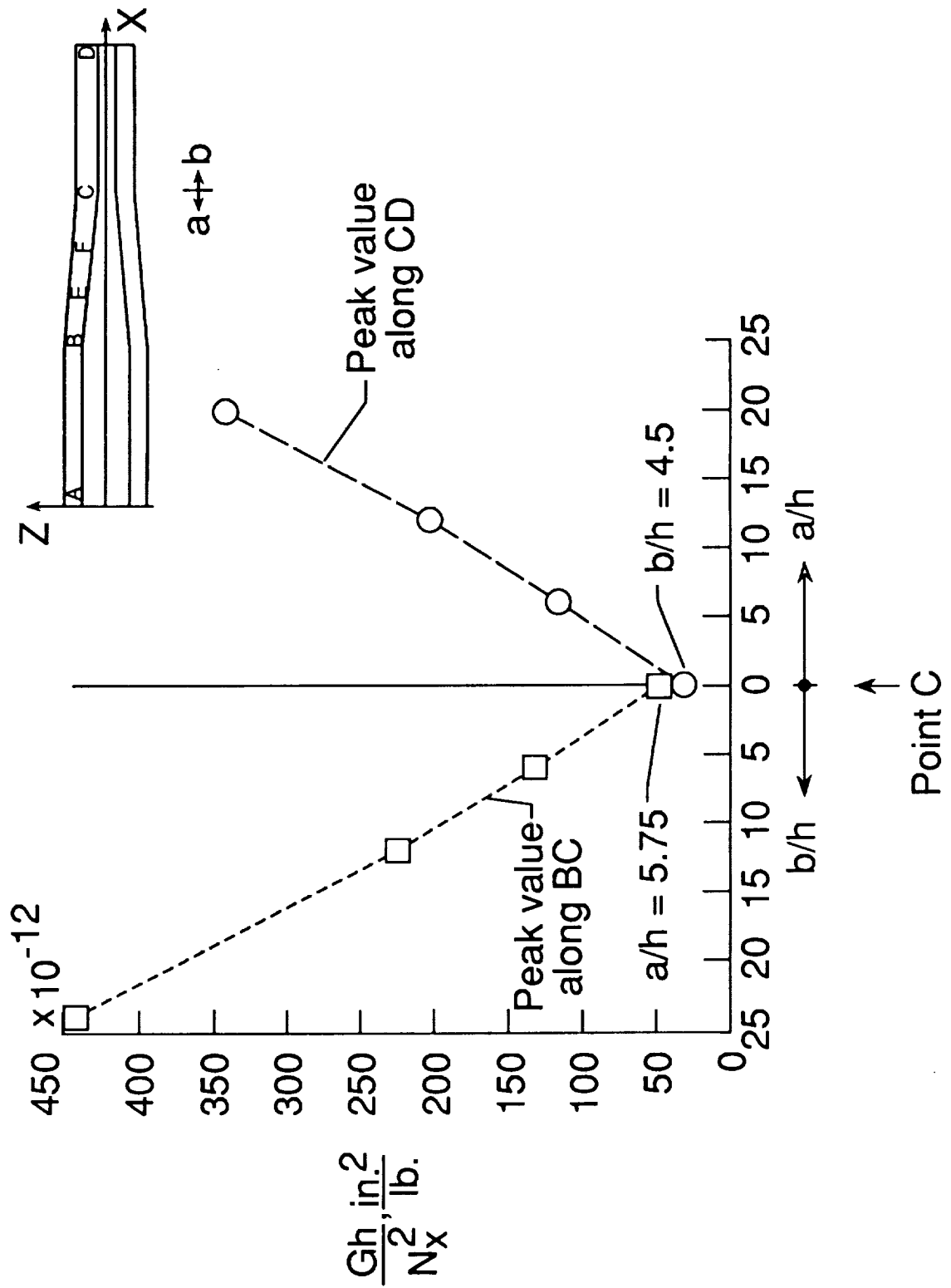
Fig. 10: Peak values of total strain-energy-release rate along either side of C
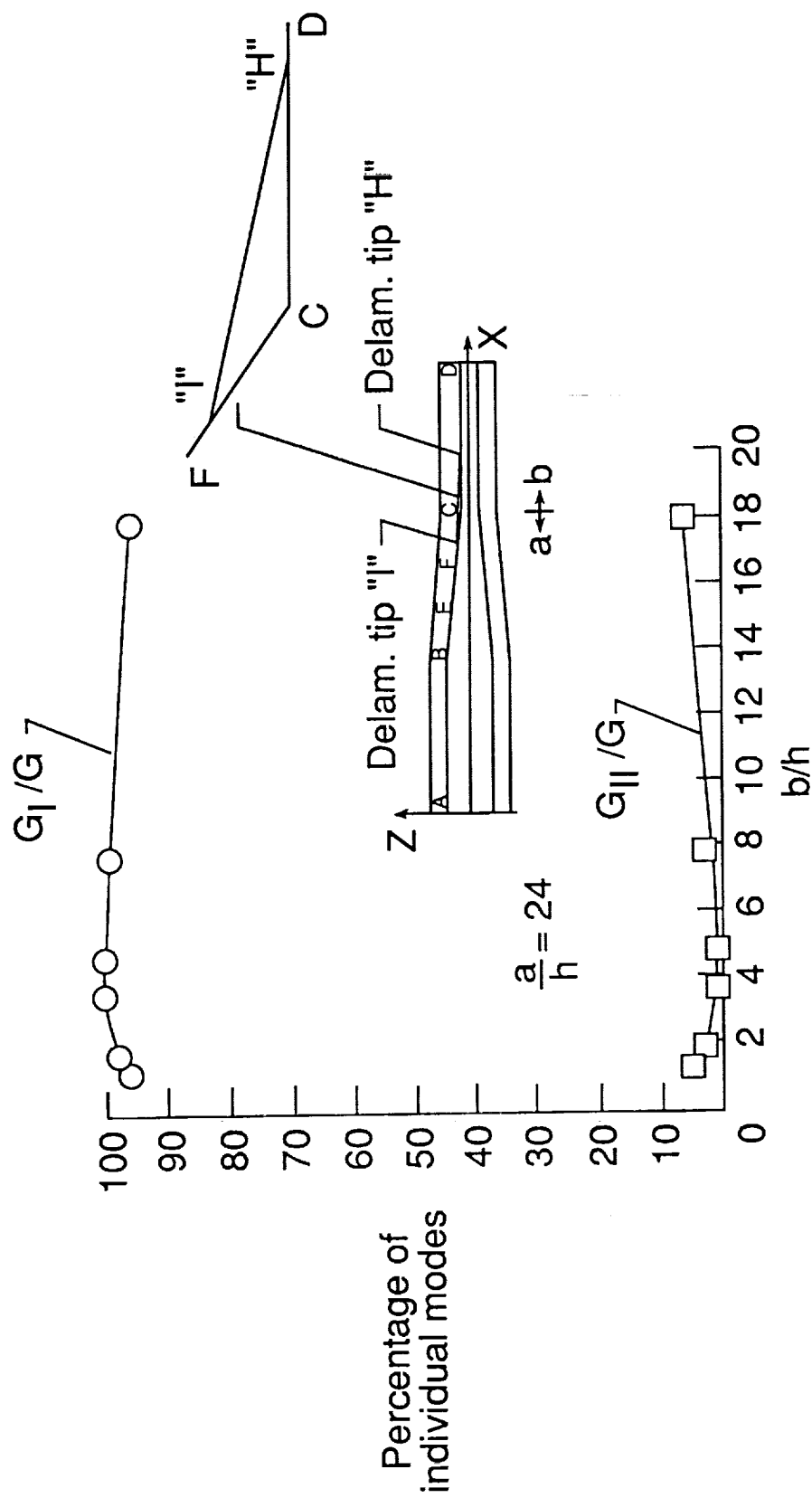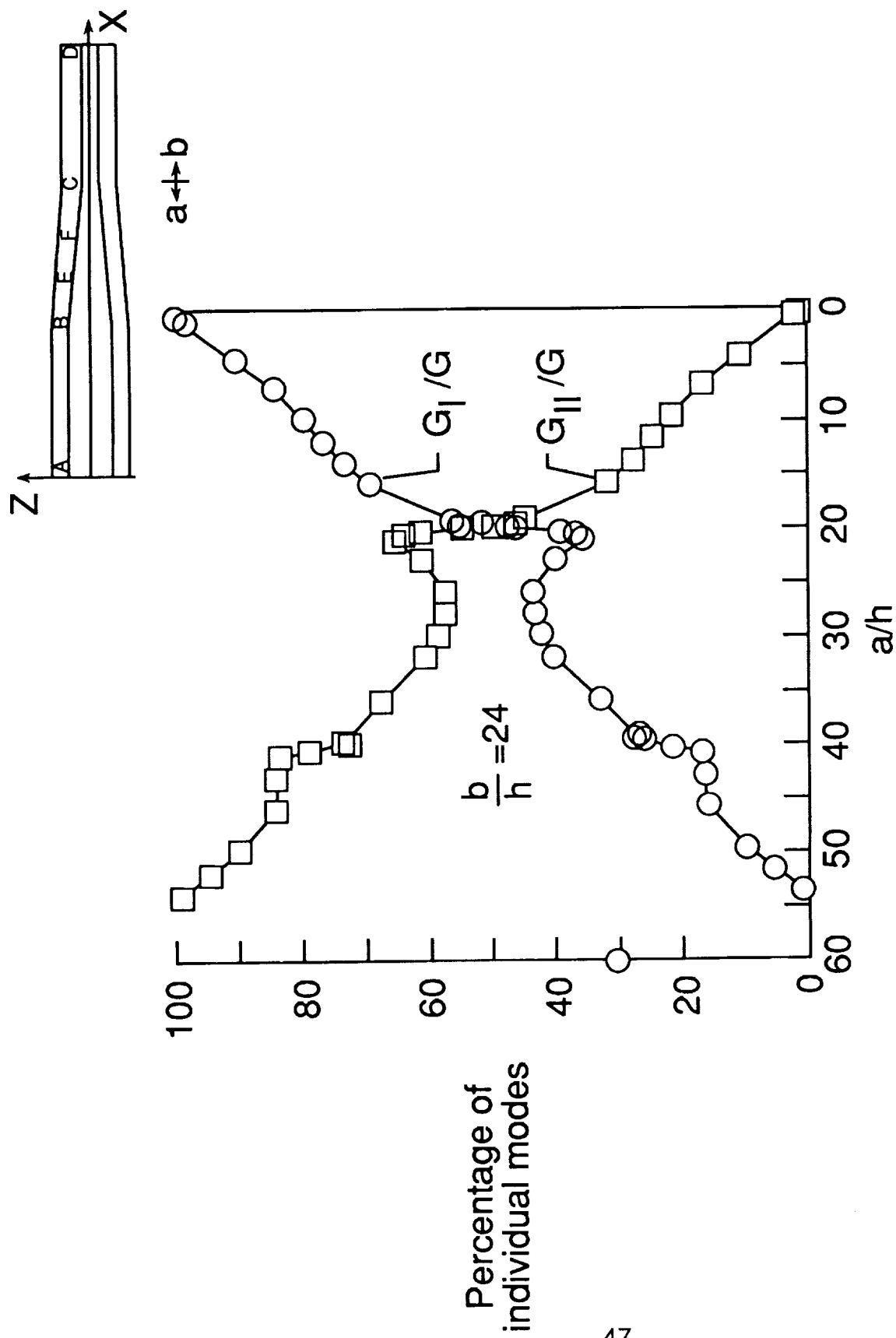
Fig. 11: G_I/G and G_{II}/G at delamination tip H along interface CD

46

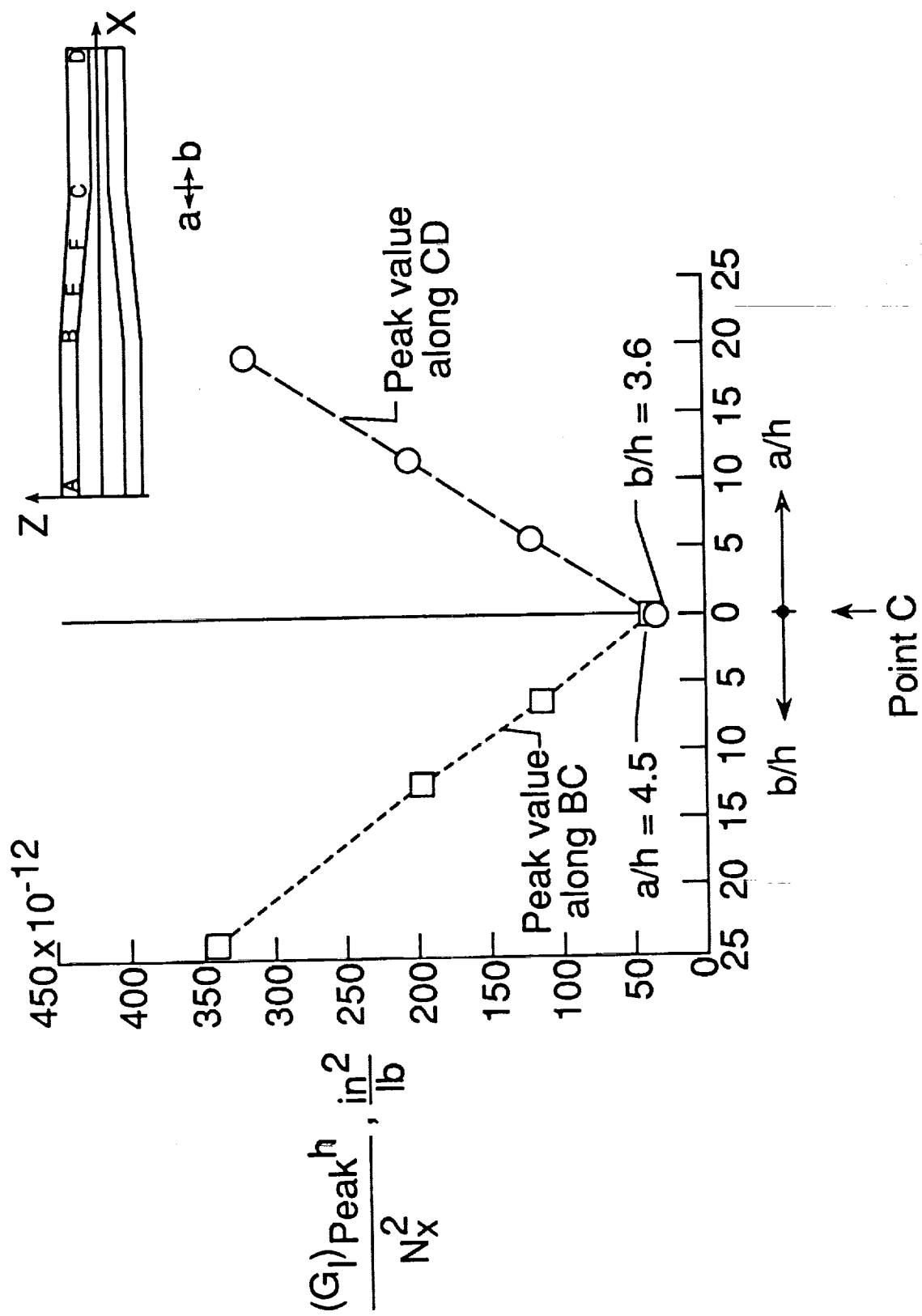Fig. 12: G_I/G and G_{II}/G at delamination tip I along interface BC
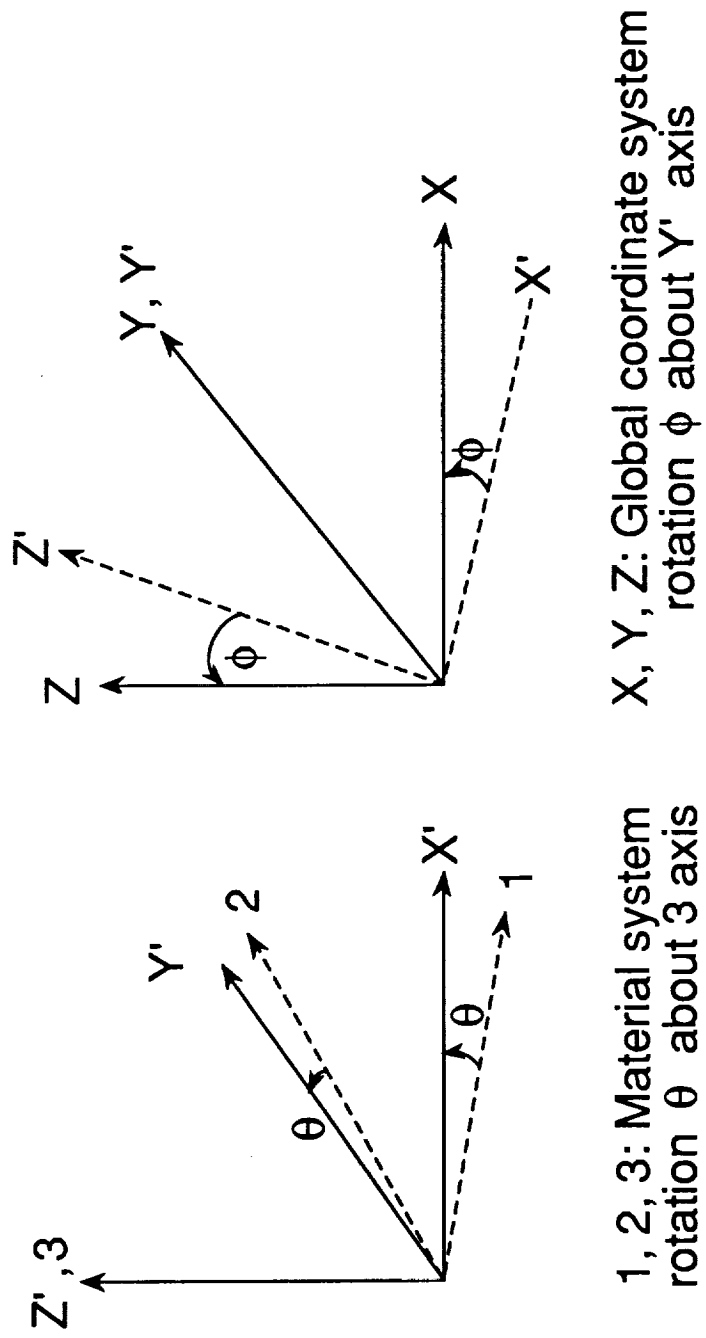
Fig. 13: Peak values of G_I on either side of C

Y', Y

Z'

Z

φ

φ

X

X'

X, Y, Z: Global coordinate system
rotation φ about Y' axis

Y'

2

X'

1

θ

θ

Z', 3

1, 2, 3: Material system
rotation θ about 3 axis

Fig. 14: Material and global coordinate systems and rotations

used in the transformations

NASA
National Aeronautics and Space Administration

Report Documentation Page

1. Report No. NASA TM-102592 AVSCOM TM-90-B-003	2. Government Accession No.	3. Recipient's Catalog No.
4. Title and Subtitle Strain Energy Release Rate Analysis of Delamination in a Tapered Laminate Subjected to Tension Load		5. Report Date March 1990
		6. Performing Organization Code
7. Author(s) S. A. Salpekar*; I. S. Raju**; and T. K. O'Brien***		8. Performing Organization Report No.
		10. Work Unit No. 505-63-01-05
9. Performing Organization Name and Address NASA Langley Research Center, Hampton, VA 23665-5225 U.S. Army Aviation Research Technology Activity (AVSCOM) Aerostructures Directorate Hampton, VA 23665-5225		11. Contract or Grant No.
12. Sponsoring Agency Name and Address National Aeronautics and Space Administration Washington, DC 20546 U.S. Army Aviation Systems Command St. Louis, MO 63166		13. Type of Report and Period Covered Technical Memorandum
		14. Sponsoring Agency Code

15. Supplementary Notes

16. Abstract

A tapered composite laminate subjected to tension load was analyzed using the finite-element method. The $\{[0_7/(\pm45)]/\uparrow[(\pm45)_3]/[0/(\pm45)/0]\}_s$ glass/epoxy laminate has a $(\pm45)_3$ group of plies dropped in three distinct steps, each 20 ply-thicknesses apart, thus forming a taper angle of 5.71 degrees. Steep gradients of interlaminar normal and shear stress on a potential delamination interface suggest the existence of stress singularities at the points of material and geometric discontinuities created by the internal plydrops. The delamination was assumed to initiate at the thin end of the taper on the -45/+45 interface indicated by the arrow in the laminate layup and the delamination growth was simulated in both directions, i.e., along the taper and into the thin region. The strain-energy-release rate for a delamination growing into the thin laminate consisted predominantly of mode I (opening) component. For a delamination growing along the tapered region, the strain-energy-release rate was initially all mode I, but the proportion of mode I decreased with increase in delamination size until eventually total G was all mode II. The total G for both delamination tips increased with increase in delamination size, indicating that a delamination initiating at the end of the taper will grow unstably along the taper and into the thin laminate simultaneously.

17. Key Words (Suggested by Author(s)) Tapered laminate Plydrop Delamination Strain-energy-release rate Two dimensional analysis	18. Distribution Statement Unclassified - Unlimited Subject Category - 24	
19. Security Classif. (of this report) Unclassified	20. Security Classif. (of this page) Unclassified	21. No. of pages 50	22. Price A03

NASA FORM 1626 OCT 86